## Recent Progress of MAFF

D. Habs, R. Krücken, M. Groß, T. Faestermann, W. Assmann, L. Beck, W. Carli, S. Emhofer, R. Großmann, P. Hartung, S. Heinz, P. Jüttner<sup>a</sup>, O. Kester, H.J. Maier, P. Maier-Komor, F. Nebel, M. Pasini, M. Schumann, J. Szerypo, P. G. Thirolf, F. Tralmer<sup>a</sup>, and E. Zech

<sup>a</sup> ZWE Forschungsreaktor München II, Garching

April 15, 2003 has been an important date to the FRM-II and also to MAFF: The German federal ministry for environment gave its o.k. for the start-up of the new reactor and on May 12, 2003 the final operating license has been granted to the FRM-II. Since then the MAFF authorization procedure could commence officially. Initiated by the experiences of the FRM-II, we are actually negotiating a full-cost quotation by the TÜV Süddeutschland for the complete expertise.

### 1. Preparatory work

A rather precise knowledge of the distribution of radioactivity within the MAFF system is of utmost importance to the layout of the system and to the specifications that will be applied. This question is closely linked to the efficiency of the in-pile cryopanels. First theoretical studies taking into account the actual geometrical conditions within the beam tube indicate that the initially assumed suppression factor of  $10^4$  (based on vacuum conductance ratios) may even be a conservative estimate.

Additional work is, however, necessary to confirm these results. Moreover, not only the fraction of activity retained by the cryopanels within the reactor beam tube is important, but also the distribution of the remaining activity along the beamline and in the vacuum system. The vacuum system itself has been revised and seems now more consistent than before making full use of the advantages of cryopumps, e.g. no open pumping lines during operation (cf. section 2.2).



 $\underline{\text{Fig. 1}}$ : The feedthrough-plug in the wall between neutron-guide hall and neutron-guide tunnel.

Progress has also been made in the design of the in-pile parts of MAFF. The new shielding plugs supporting the cryopanels as well as the source or lens trolley are meanwhile in a stage of rather detailed design. The same is true for the trolleys; the beam extraction system on the lens trolley permits the necessary beam adjustments to correct

a transversal offset between source trolley and lens trolley (see 2.3).

The feedthrough-plug in the wall between neutron-guide hall and neutron-guide tunnel has been installed on schedule as shown in figure 1.

# 2. Development of components and subsystems

#### 2.1 Cryopanel

A considerable fraction of the radioactivity produced in the MAFF fission target will consist of short-lived gaseous activity, like krypton or xenon fission products or the halogens bromium and iodine. It is intended to prevent migration and release of these volatile fission products by localizing them on a He-cooled cryopanel until transformation into non-volatile species by  $\beta$  decay. The required operational temperature below 20 K results from the vapour pressures of the gases and vapours that have to be pumped. At this temperature the usual rest gas components (except hydrogen) as well as the fission isotopes of Kr, Xe, Br, I will be frozen at remaining vapour pressures in the UHV region  $(\leq 10^{-11} \text{ mbar})$ . Such cryopanels will be installed in the MAFF beamtube at either side of the fission source (SR6-a and SR6-b). Limited by the inner diameter of the beamtube (250 mm) as well as by the MAFF fission source required to be moved inside the cryopanel, a compact design had to be developed. As an adequate solution a doublewall tube (gap width 4 mm) with 6 spiral-like separated sections for in- and outlet of the cold He gas was designed. The cryopanel length is 1 m, the inner diameter of the He double-tube amounts to 157 mm, the minimum value needed still to be able to move the fission source inside the cryopanel. The wall thickness of 2 mm is a compromise between the safety regulations for a pressure vessel on the one hand and the minimization of the nuclear heating due to the neutron and  $\gamma$  flux. A passive floating heat shield will reduce the thermal heat load form the surrounding warm beam tube. Aluminum of the type 6061-T6 was chosen as material for the cryopanel because of its cryogenic specifications needed for the operation at an input temperature of 10 K, while the output temperature will be about 20 K. In addition material specifications and certificates for the use in a nuclear reactor environment already exist for Al 6061-T6.

The cryopanels will additionally provide the necessary high-vacuum conditions close to the fission source. The pumping capacity of the cryopanels is depending on the pressure and the gas type, amounting to about  $12.7~\rm l\,s^{-1}\,cm^{-2}$  for nitrogen and  $5.9~\rm l\,s^{-1}\,cm^{-2}$  for xenon. The overall pumping capacity of the cryopanels on each side of the beam line will amount to about  $8\cdot10^4\,\rm l\,s^{-1}$  for nitrogen and  $4\cdot10^4\,\rm l\,s^{-1}$  for xenon.

In order to build up the technological knowledge for

manufacturing the cryopanel via cryogenic shrinking and to allow for performance tests, a prototype has been produced by ACCEL (Bergisch Gladbach), which is shown in Fig. 2. It has been installed in the MAFF test beamline at the MLL and has been coupled via a new Helium transfer line to the Helium refrigerator, thus allowing to start an extensive test programme to characterize the performance of the cryopanel.



Fig. 2: Prototype of the MAFF cryopanel.

#### 2.2 Vacuum system

In the Annual Report 2002 the new design of the vacuum system of the low energy MAFF beam tube was introduced. The new concept bases on refrigerator cryopumps (DN 160) for producing and maintaining high vacuum. As roughing pumps and for regeneration of the cryopumps dry pumps are foreseen. Since such cryopumps are usually not designed to withstand overpressure, they cannot be directly attached to the MAFF reactor beam tube which is designed to withstand a maximum pressure of 6 bar in case of a severe failure scenario. Therefore the cryopumps must be pressure-isolated from the reactor beam tube by fast closing gate valves and shock isolated by bellows-type compensators. The fast closing valves of the required size have a closing time of  $\approx 25$  ms which is too long to prevent venting of the cryopump and do not withstand a differential pressure of 6 bar. Therefore it was decided to make the cryopumps part of the beam tube unit which is designed to preserve its integrity in case of failures. Therefore a special cryopump has been designed in cooperation with LEYBOLD VACUUM. The pump casing is reinforced to withstand 6 bar, the safety valve for gas discharge and the fore-vacuum flange are not required and thus with the exception of the main port and the electrical feedthrough for the temperature sensor the cryopump has no flanges. The required fore-vacuum flange for regeneration is included in the modified gate valve (DN 160) for the cryopump. This type of gate valve (VAT) is designed with a thicker wall for the body and stiffer bellows to meet the requirements for an accident with overpressure up to 6 bar. In this type of setup the bellows type shock absorbers are not required because the cryopumps with their gate valves are part of the system designed for integrity.

Volatile fission products (Kr, Xe, Br and I) migrate in the whole vacuum system. Most of them stick to the inpile cryopanel  $(T \approx 15 \text{ K})$ , the rest is trapped in the cryopumps. When the cryopanel is warmed up the portion of the volatile fission products which have not transformed so far by  $\beta$ -decay into non volatile atoms are released again and migrate in the high vacuum system until they are trapped in one of the active cryopumps. Even the longest living bromine isotope (83Br;  $T_{1/2} = 2.4 \text{ h}$ ) decays completely after one reactor cycle of 52 days. In case of iodine only <sup>129</sup>I is problematic due to its long lifetime of  $> 10^7$  a. Since the iodine fission product concentration is very low — no iodine atom will meet another one — the chemical sorption will be perfect to any wall. Thus only noble gas fission products with longer half-lifes must be taken into consideration. The longest living xenon isotope  $(^{133}\text{Xe}; T_{1/2} = 5.25 \text{ d})$  decays completely after a few reactor cycles. Only the longest living Kr isotope (85Kr;  $T_{1/2} = 10.76$  a) largely remains in the second stage of the cryopump. With the assumption that about 0.235 g of the <sup>235</sup>U in the MAFF ion source fissions during one reactor cycle and the isobaric yield of  $^{85}\mathrm{Kr}$  is  $1.327\,\%$  a  $^{85}\mathrm{Kr}$  load of 0.3 mbar·l would be stored in one cryopump. If we further assume that the pumping capacity for Kr is the same as the measured one for He (which is an underestimation) the MAFF ion source could be pumped by one cryopump for more than 300 years. Unfortunately, the MAFF ion source emits CO synthesized by the dominant partial pressure of H<sub>2</sub>O on its up to 2400 K hot graphite and carbide material. Fortunately the amount of CO seems to be of the same order of magnitude as the long living noble gas fission products. Therefore regeneration of the cryopumps will only be required if some leakage arises due to malfunction. It is not likely that during regeneration with a typical vacuum of 0.1 mbar at maximum, aerosols with solid radioactive fission products are formed. Nevertheless, we want to improve the filtering of the exhaust gases which finally will be released into the exhaust gas system of the reactor (KLA 70) after passing a mechanical filter for grain sizes  $> 0.1 \,\mu\mathrm{m}$  with an efficiency of 99.99%. For this purpose we will develop a slow filter which gases can pass only by diffusion. The gases released from the cryopump are transported by a dry roughing pump into a decay tank (Fig. 3), where they are stored for several reactor cycles. The decay tank with an initial pressure < 1 mbar is filled by several regeneration cycles up to 300 mbar. For a subsequent regeneration of cryopumps a second decay tank can be filled. In order to empty the first decay tank, it will be connected to the secondary tank via the slow diffusion filter. The pressure in the secondary tank is slightly lower ( $\Delta p \approx 20 - 50 \text{ mbar}$ ). Thus the pressure in both tanks equalizes via the slow diffusion filter only during longer time periods. Turbulent flow which might create aerosols is such suppressed and the gas diffusion through the filter is not forced, thus solid particles trapped in the filter cannot be set free to reach the other side of the slow filter. When pressure equilibrium is reached, the valves between decay tank and slow filter are closed and by means of the dry roughing pump the required initial differential pressure between both tanks is produced again before the decay tank is further drained via the diffusion filter. The gas of the secondary tank is then exhausted by a dry vacuum pump via a mechanical filter into KLA 70. The transfilling cycles from the decay tank to the secondary tank are repeated until the decay tank is empty.

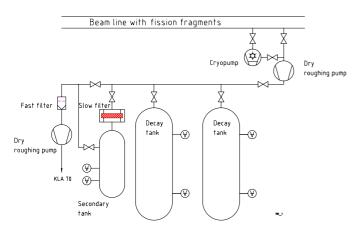


Fig. 3: Decay tanks of the MAFF vacuum system with slow diffusion filter.

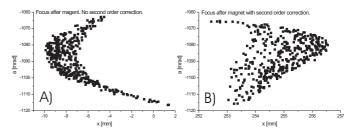
#### 2.3 Beam transport

In order to gain a better understanding of the design of the beam transport devices from the ion source to the beam cooler, simulations with SIMION7 have been carried out. SIMION is using a numerical approach to solve the Laplace equation and is therefore an improvement of the previously made first order COSY calculations. For the SIMION simulations the whole beam line from the ion source up to the cooler has been modelled. The transport of the 30keV beam has been optimized with respect to transmission and emittance. Furthermore several crucial issues have been addressed for the first time.

Of utmost importance was to study the effect of a transversal offset between the ion source exit and the beam transport entrance hole. Source and extraction electrodes are moved into the reactor tube on different trollies from both tube ends. Although aligned by mechanical means a worst case offset of up to 5 mm seems possible. Two transversal deflections are required to bend the beam back on axis. The first deflection is achieved by applying voltage to a four fold segmented extraction electrode. This electrode has a 15 mm diameter hole in order to guarantee maximum transmittance even for large offsets. Finally the beam direction is corrected by a second steerer installed in the first quadrupole triplet. With appropriate steering voltages, almost no emittance growth is visible. The x and y emittances stay at about  $12 \pi$  mm mrad at the entrance of the first electrostatic deflector.

Due to its own weight the unsupported end of the beam tube is bending downwards by approximately 1.9 mm. This effect can be corrected with the triplets steering capabilities.

Conclusively it can be stated that offsets due to mechanical imperfections can be corrected with the available steering possibilities.



<u>Fig. 4</u>: Emittance after the magnet: a) without shunts, b) with shunts.

In a second step the beam line was extended up to the ion cooler, adding a  $31.5^{\circ}$  electrostatic deflector, an  $80^{\circ}$  dipole magnet and two other quadrupole triplets. One between the magnet and a  $60^{\circ}$  electrostatic deflector, the second one after the deflector.

Studying the emittance development throughout the various instances it became apparent, that  $31.5^{\circ}$  is a crucial value for the first deflection angle and that the beam picks up a large distortion by passing through the electrostatic deflector, which results in a crescent shaped sextupole abberation after the magnet as can be seen in fig. 4 a). In general this error could be corrected by a sextupole lens or by adding a pair of shunts to the electrostatic dipole, with the entrance shunt being curved. The shunt solution resolves in a significant reduction of the sextupole abberation as can be seen in fig. 4 b). Further downstream, x emittance grows after the  $60^{\circ}$  deflector to almost  $50 \, \pi$  mm mrad, even though the same sextupole correction is applied. No extensive studies of this increase have been carried out since  $100 \, \%$  transmittance to the cooler can be maintained.

Simulations done by Sophie Heinz show that the increased emittance can be handled by the cooler.

#### 2.4 Accelerator

For the MAFF accelerated radioactive ion beams facility [1] a new layout has been proposed in order to fulfill new experimental requirements and space availability [2]. The main feature added to the previous layout is the possibility to install an external multi-harmonic buncher upstream the RFQ, with a fundamental frequency of 12.66 MHz, which allows a time separation between bunches of about 80 ns.

The first acceleration stage consists in an IH-RFQ operating at 101.28 MHz frequency and at maximum duty cycle of 10%. The MAFF IH-RFQ will accelerate ions with A/q < 6.5 from 30 keV injection energy up to 300 keV/u. Downstream the RFQ a cleaning section is also foreseen in order to improve the beam quality especially in the time domain. The following acceleration chain consists in a 101.28 MHz 2 m long IH DTL, which boosts the energy up to 1.45 MeV/u and in four 202.56 MHz IH-DTLs where the energies increments are 3.0, 4.2, and 5.4 MeV/u, respectively. Finally there are two small 7-gap resonators which are used to vary continuously the energy between 3.6 and 5.9 MeV/u. Fig. 5 shows the global layout of the experimental facility.

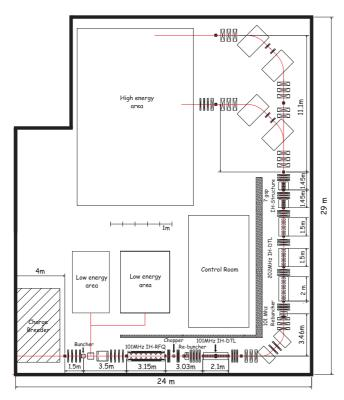
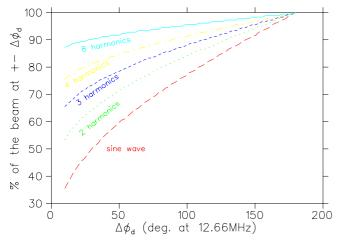
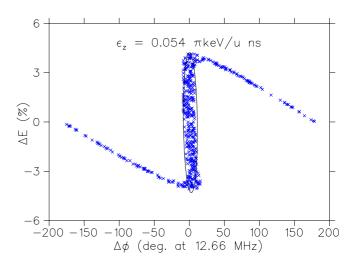


Fig. 5: Layout of the experimental area.

Due to the very low voltages requirements (less than 200 V), the multi-harmonics buncher can be realized by means of a pair of circular parallel plates where an electrical tension is applied directly for every single harmonic. This kind of configuration does not require any kind of resonant structure and can be made very easily. A study analysing the bunching efficiency together with particle tracking has been done for the MAFF case and results can be found in [3]. As a summary we include here in Fig. 6 a plot of the several bunching efficiencies for different numbers of harmonics, and also in Fig. 7 a plot of the longitudinal phase space of the beam 1 m downstream the buncher itself.



<u>Fig. 6</u>: In this plot the efficiencies are calculated as the percentage of beam enclosed in a  $\Delta\phi=\pm\phi_d$  after some distance d



<u>Fig. 7</u>: Longitudinal phase space portrait of the beam ready for injection into the RFQ.

In Fig. 7 the energy spread is the required one to produce a focus 1 m after the buncher. In order to allow a good capture inside the RFQ, this energy spread has to be reduced and hence the length in between has increased to 3.5 m (as shown in Fig. 5).

As for the RFQ a new beam dynamics has been determined. A new set of machine parameters is listed in Table 1.

Frequency $f$	$101.28~\mathrm{MHz}$
Voltage	70  kV
Length	2810 mm
r0 parameter	$4~\mathrm{mm}$
minimum aperture	$2.9 \mathrm{mm}$

<u>Table 1</u>: Beam Dynamics parameters

The RFQ dynamics was optimized in order to get as high transmission as possible in the double configuration of pre-buncher on/off. In all cases the transmission has been simulated higher than 99 % and the beam was always transported through the end of the RFQ. This is very important in case of a very intense beam because we can localize all the residual losses in the following cleaning section thus reducing the maintenace risks due to activation.

Simulation of the electromagnetic properties of the resonator has been performed with MWS [4] and an optimized geometry has been proposed in [5]. The calculation performed with the code MWS has shown significant differences in the shunt impedance and in the power dissipation with respect to the results obtained with MAFIA. The differences are due to the different meshing procedure for a given boundary condition and the accuracy of the results depends significantly on the simulation technique [6]. In order to test the calculations with MWS we have built a short model in aluminum shown in Fig. 8 to check the resonant frequency, to test the bead pull measurements and to verify the frequency tuning range. As for the measurement of the resonance frequency we have an estimated error of  $<0.5\,\%$ .

Table 2 shows a summary of the electrical properties calculated for the real RFQ.

Q-value	7932
Shunt Impedance $R_p$	$196~\mathrm{k}\Omega\mathrm{m}$
Flatness of the ref voltage	< 1.5%
Vertical dipole component $\alpha$	< 1.5%
Power on the electrodes	12.1%
Power on the stems	36.8~%

Table 2: RF parameters and power distribution of the IH-RFQ

As for the real resonator, progress has been done in the mechanical construction. The whole cavity will be splitted into 5 identical central modules each 400 mm long and 2 end modules 430 mm long. These modules will be made from bulk copper cylinders. Particular care has been dedicated to reduce the number of brazing procedures and hence the cost of the cavity itself. A request for offer has been sent out and three firms have been indicated as capable to construct the resonator.

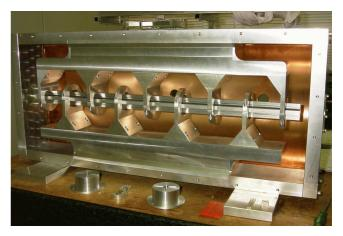


Fig. 8: Aluminum model of the resonant cavity.

#### References

- O. Kester et al., The Munich Accelerator for Fission Fragments (MAFF), AIP Conf. Proc. 473 (1998) 536
- [2] M. Pasini et al., Radioactive Ion Beam Acceleration ar MAFF, to be published in Nucl. Phys. A
- [3] M. Pasini Pre-RFQ Buncher Studies, Notes on the Multi Harmonics Buncher for MAFF
- [4] Micro Wave Studio, CST Computer Simulation Technology http://www.cst-world.com/
- [5] T. Sieber, Ph.D. thesis, LMU München, 2001
- [6] M. Pasini, Notes on MAFF IH-RFQ simulation with MWS